Astron. Astrophys. 332, 1055–1063 (1998)

ASTRONOMY AND ASTROPHYSICS

Near infrared imaging and spectroscopy of the IRAS 20126+4104 region⋆

S. Ayala[1], **S. Curiel**[1], **A.C. Raga**[1], **A. Noriega-Crespo**[2], **and L. Salas**[3]

[1] Instituto de Astronomía, UNAM, Ap. 70-264, 04510 México, D.F., México
[2] Infrared Processing and Analysis Center, CalTech-JPL, Pasadena, CA 91125, USA
[3] Instituto de Astronomía, UNAM, Ap. 877, 22830 Ensenada, México

Received 22 August 1997 / Accepted 6 January 1998

Abstract. In this paper we present near-infrared images and K′-band spectra (1.95-2.30 μm) of the nebulae located in the IRAS 20126+4104 region. We find bright cometary shaped objects to the Northwest of the IRAS position and other emission line objects to the Southeast. We have detected 6 low excitation emission lines of molecular hydrogen, and present spatially resolved excitation temperatures, 1-0 S(1)/2-1 S(1) line ratios and ortho-para ratios for the brighter emission line objects near the IRAS source. The integrated flux in the H_2 1-0 S(1) line of the brighter object located to the Northwest of the IRAS position is $6.85 \times 10^{-13}\ erg\ cm^{-2}\ s^{-1}$, integrated within an aperture of $10.2\, arcsec^2$. From a spectrophotometric analysis, we conclude that the H_2 emission observed in this nebula is mainly produced by collisional excitation combined with fluorescent H_2 emission. However, it is unclear from our observations whether the UV radiation field that would be responsible for the fluorescent component is produced by the IRAS source itself, or by the stars embedded at the Eastern edges of two of the observed condensations.

Key words: ISM: jets and outflows – infrared: ISM: lines and bands – ISM: individual objects: IRAS 20126+4104

1. Introduction

In recent years, shocked molecular hydrogen (H_2) emission has been found in association with Herbig-Haro objects and/or with molecular outflows, suggesting that these manifestations of the outflow phenomenon are closely related.

At the present time, the relationship between the highly supersonic collimated gas (optical and/or NIR jet) and the slower, denser and less collimated molecular outflow seen mainly in CO, SiO and HCO^+, as well as the nature of the excitation of the molecular emission observed in the NIR are not clear. The scenarios which have been proposed to explain this relationship fall into two main groups: two-wind models, and unified models. In the former, the supersonic jet arises from a stellar wind, while the slower and less collimated molecular outflow arises from an accretion disk. In the latter, the jet provides the necessary momentum to drive the molecular outflow, either by displacing jet gas sideways in a 'wake' (Raga and Cabrit 1993) or by sweeping up molecular gas in 'shells' (Chernin & Masson 1993).

Direct imaging of molecular outflows has revealed a variety of morphologies in the H_2 line emission, including compact structures, filamentary jet-like structures or sweeping bow shocks; and in several cases diffuse, extended structures. Spectroscopic studies of the near infrared (NIR) H_2 emission in molecular outflows show that the molecular hydrogen is thermally excited, probably in molecular shock waves (e.g., Gredel 1994; Schwartz et al. 1995). However, in some cases the H_2 upper vibrational levels appear to be excited by fluorescence (e.g., Fernandes & Brand 1995; Fernandes, Brand & Burton 1996). The molecular lines produced by collisionally excited H_2 molecules are typically characterized by an excitation temperature $T_{exc} \sim$ 2000–3000 K, while in the cases where the upper vibrational levels are contaminated by fluorescence, the observed lines cannot be explained with a single excitation temperature.

IRAS 20126+4104 is situated in a dark globule in the Cygnus-X -region at a distance of 1.7 kpc. This source is associated with a high-velocity molecular outflow roughly oriented in the North-South direction (Wilking, Blackwell & Mundy, 1990). Based on its far-infrared colour characteristics, this IRAS source has been classified as an ultracompact (UC) HII region (Bronfman et al. 1996, Molinari et al. 1996). In the near-infrared, this region has been observed in the K′-band by Hodapp (1994), who found a bipolar nebulosity close to the center of the outflow, which is embedded in a more extended, diffuse nebulosity. More recently, Cesaroni et al. (1997) found a compact, bipolar molecular outflow in HCO^+ and CS in the SE-NW direction, as well as extended NIR H_2 line emission and continuum structures, nearly aligned with this outflow. They also found a compact 3-mm continuum source located close to its center. This radio continuum source was also detected at centimeter wavelengths by Martí and Rodríguez (1997), showing that its spectral index is consistent with optically thick free-free emission at centimeter

Send offprint requests to: S. Ayala (sayala@astroscu.unam.mx)

⋆ Based on observations obtained at the Observatorio Astronómico Nacional at San Pedro Mártir, B.C. México

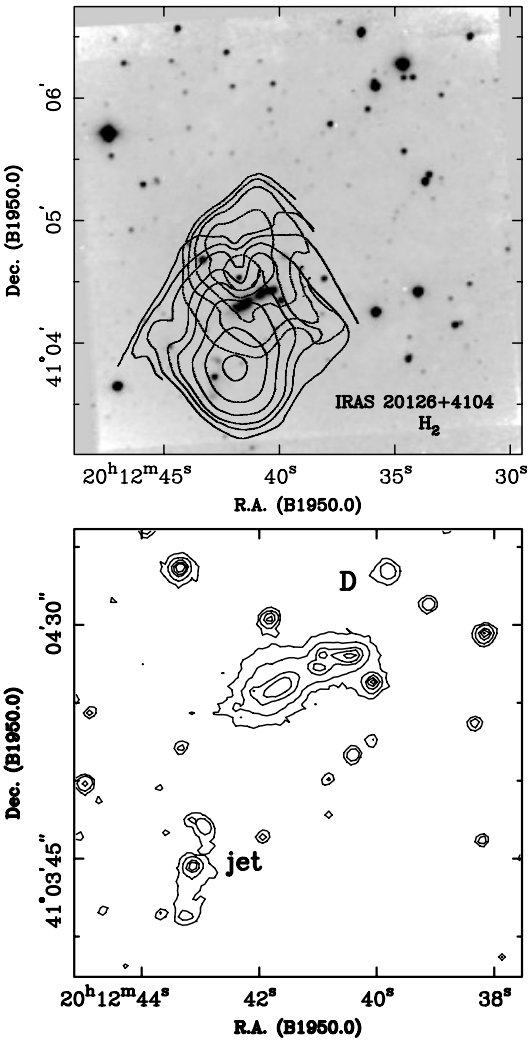

Fig. 1. *Top:* Map of CO integrated intensity (Wilking el al. 1990) overlaid on a grey-scale H_2 1-0 S(1) (+ continuum) low resolution image of the region around IRAS 20126+4104. The Northern lobe corresponds to the blue-shifted molecular gas and the Southern lobe to red-shifted gas. *Bottom:* Contour map of a close up around the IRAS source of the H_2 1-0 S(1) image. The values of flux for each contour are: 0.7, 2, 8, 16 and 30$\times$ 10^{-16} $erg\ cm^{-2}\ s^{-1}\ arcsec^{-2}$.

wavelengths, and with optically thin dust emission at millimeter wavelengths (see also Cesaroni et al. 1997). This radio source is deeply embedded in a dense molecular core observed in ^{13}CO, CS, CH_3CN and CH_3OH, and has a number of H_2O maser spots coinciding with it (Cesaroni et al. 1997). These characteristics indicate that the powering source of this bipolar outflow is associated with a very young B2.5–B0.5 star.

We present narrow-band H_2 and broad-band K′ images with high spatial resolution around this IRAS source. These images show two bright nebulae with cometary morphology, apparently associated with embedded stars. We discuss the origin of the excitation of the H_2 line emission based on low resolution spectra taken along these extended structures.

Table 1. Filters and exposure times used in direct image observations

filter	λ $[\mu m]$	$\Delta\lambda$ $[\mu m]$	$t^{\dagger}_{exp}$ [sec]
K´	2.125	0.35	480
H_2 1-0 S(1)	2.122	0.02	720
cK	2.260	0.06	450

† Total exposure time at the center of each mosaic.

2. Observations

Imaging and spectrophotometric observations were carried out during 5 consecutive nights in August 1996 using the near-infrared camera/spectrograph CAMILA (Cruz-González et al. 1994) on the 2.1m telescope of the Observatorio Astronómico Nacional (at San Pedro Mártir, Baja California, México). The camera/spectrograph has two cameras with f/4.5 and f/13.5 (hereafter "low resolution" and "high resolution" cameras, respectively), equipped with a 256×256, 24μm pixel NICMOS3 array. The low and high resolution modes yield 0.85 ″/pixel and 0.3 ″/pixel scales, respectively.

We obtained several images and spectra of the IRAS 20126+4104 region through H_2, cK and K′-band filters. Both images and spectra were reduced using standard sky subtraction and bad pixel removal techniques with IRAF-based programs. The images were processed by subtracting a median-filtered image of nearby sky frames taken with the same integration time and with an offset of about 1.5′ from the IRAS source position. The images were flattened by a combination of low and high illumination sky flats obtained at sunset. For each filter, mosaics were made with frames containing the IRAS region, which were then aligned using several field stars. Finally, we estimated the plate scale and the orientation of the images using 7 optically visible stars in the Digitized Sky Survey, obtaining a positional uncertainty of $\simeq$1″.

In Table 1 we present the width and central wavelength in microns of the filters used, as well as the total integration times for the final mosaic images. The total integration times correspond to the overlapping areas toward the center of our narrow-band mosaics. Fig. 1 shows our low resolution H_2 1-0 S(1) + continuum image, in grey scale, which is discussed below.

For the near-infrared K′-band spectra (1.95-2.30 μm), we employed the f/4.5 camera and a slit of 1.5″ width and 22″ length, giving a spectral resolution of R=$\lambda/\Delta\lambda$=500 in K′. Initially, the slit was oriented E-W in order to intersect the brightest object located NW of the IRAS 20126+4104 position (labeled "1" in figure 2a). The total exposure time for the final spectrum in this position was 10 minutes. We also obtained several spectra for two slit positions separated by 1.5″ in declination (labeled "2a" and "2b" in figure 2a) with a PA$=118.7^{\circ}$ position angle, measured counter clockwise, covering most of the nebula located to the SE of the IRAS position. Each spectrum has a 2 minute integration time. For each setting, explicit sky observations were obtained. We constructed a spectrum with 12 minutes of total integration time by adding the spectra obtained through slits 2a and 2b.

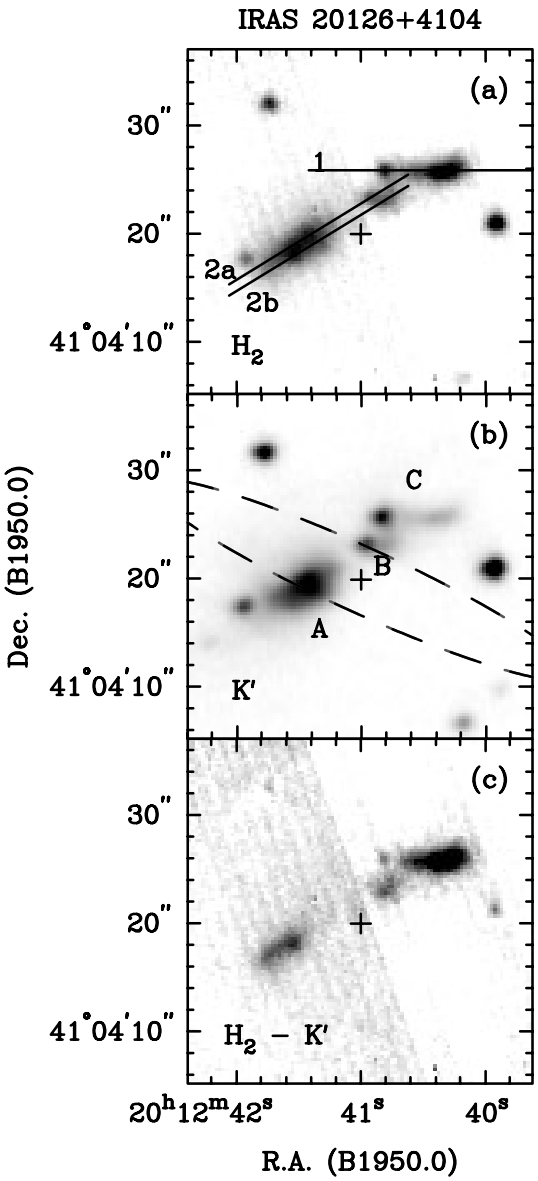

Fig. 2. a Grey-scale subsection of the high resolution H_2 at 2.12 μm (+ continuum) image of the region around IRAS 20126+4104. The slit positions for the spatially resolved spectra discussed in the text are shown. The IRAS source position is marked with a cross. **b** K′band image of the same region, showing the uncertainty in the IRAS source position with a dashed ellipse. The objects discussed in the text are labeled. **c** The H_2 continuum subtracted image. It is remarkable that line emission still remains from the star to the East of object C, and also for the star Southwest of this object.

The wavelength calibration was performed using exposures of an Argon lamp. The absolute flux calibration was achieved through observations of SA94-242 (UKIRT faint standard list) and HD 201941 (Elias et al. 1982), both early type standard stars. For the correction by atmospheric absorption we used the early type star HR 7628. The conversion factor from counts to flux was determined as a correspondence between the counts and flux per unit wavelength in the central wavelength of the K′ filter, using the standard spectra corrected for atmospheric absorption. Errors in the absolute flux calibration are around of 10% for the brighter emission lines detected. Since the lines are not resolved in our spectra, velocity shifts along the slits are not detected. The narrow and broad band mosaics were calibrated in flux using the K′ spectrum for the brightest object (slit 1). In each mosaic, we integrated the "flux" in counts/sec inside the region covered by the spectrograph slit. We then computed a conversion factor between this "flux" and the integrated flux density in the wavelength range that corresponds to the bandpass of each filter (see Table 1).

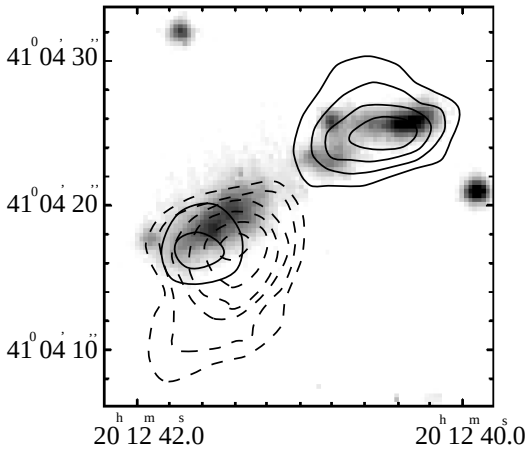

Fig. 3. Map of HCO^+ integrated intensity (Fig. 7 of Cesaroni et al. 1997) overlaid on a grey-scale H_2 1-0 S(1) (+ continuum) high resolution image. The continuous contours represent the blue-shifted lobe, and the dashed ones the red-shifted emission.

3. Results

3.1. The morphology

The multi-wavelength emission around the IRAS 20126+4104 source shows a very complex structure. Wilking et al. (1990) have detected a N-S bipolar CO outflow, with a total angular extent of $\approx 1.5'$. This outflow appears to be centred on a position $\approx 10''$ to the SW of the IRAS source. Fig. 1 (*top*) shows this outflow overlaid on an H_2 image, where the Northern lobe corresponds to the blue-shifted gas and the Southern lobe to the red-shifted gas.

Cesaroni et al. (1997) have detected an HCO^+ outflow in the same region, oriented in a NE-SW direction, with a total angular extent of $\approx 20''$. We show an overlay of this outflow on our H_2 1-0 S(1) high resolution image in Fig. 3. This outflow is centred on the nominal position of the IRAS source, which also coincides with a compact molecular core and a compact radio continuum source detected at mm/cm wavelengths (Cesaroni et al., 1997; Martí & Rodríguez, 1997).

On the $3.6' \times 3.6'$, H_2 1-0 S(1) line (+ continuum) narrow-band image shown in Fig. 1, there are three bright nebulous objects located very near to the IRAS 20126+4104 position, which have previously been reported (Hodapp 1994; Cesaroni et al. 1997; Ayala et al. 1997). The brightest object (labeled C in figure 2) has an integrated flux in the H_2 1-0 S(1) line of

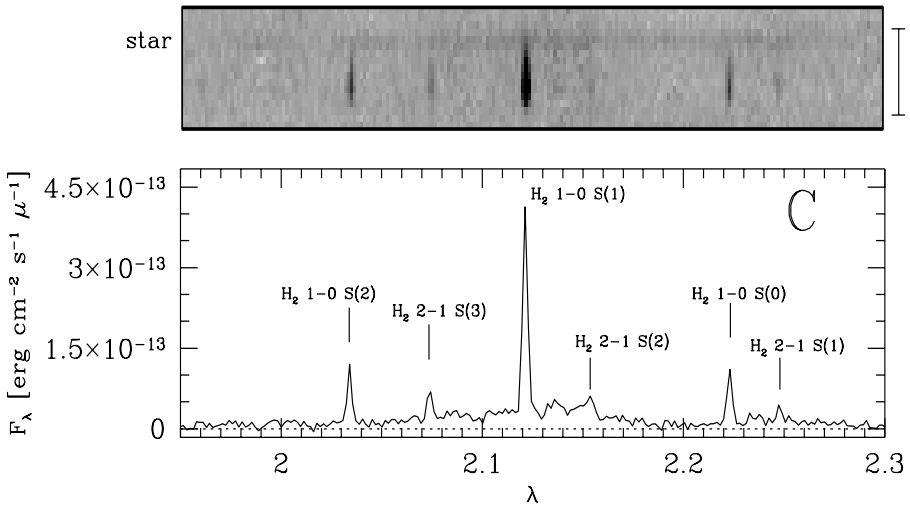

Fig. 4. *Top:* Grey-scale image of the long-slit K′-band spectrum for object C (slit 1). The aperture used to extract the spectrum (shown below) and the position of the star are indicated on the sides of the box. *Bottom:* Spectrum of object C integrated in an aperture of 11.1″ along the slit. The measured H_2 emission lines are identified.

$6.4\times10^{-13}\,erg\,cm^{-2}\,s^{-1}$ in an aperture of $10.2\,arcsec^2$, and its surface brightness is $6.2\times10^{-14}\,erg\,cm^{-2}\,s^{-1}\,arcsec^{-2}$. This object appears to be brighter than HH objects such as HH43, which has a flux in the same line of $5.20\times10^{-13}\,erg\,cm^{-2}\,s^{-1}$ in an aperture of $77.4\,arcsec^2$ and has a surface brightness of $6.72\times10^{-15}\,erg\,cm^{-2}\,s^{-1}\,arcsec^{-2}$ (Gredel, 1994). Condensation C has a cometary morphology, and appears to be connected with the star located at the Eastern end of the object; the flux presented above for condensation C does not include the stellar emission. Condensation B is smaller and fainter than C, with a cometary morphology and a weak embedded star at its Eastern edge. Its surface brightness in the H_2 1-0 S(1) line is $3.9\times10^{-14}erg\,cm^{-2}\,s^{-1}\,arcsec^{-2}$.

Two more interesting objects appear in our H_2 1-0 S(1) image. An object with compact morphology located Northwest of the IRAS source (20:12:39.8 +41:04:42, 1950; labeled D in figure 1), which is not detected in our cK image, indicating that it is an emission line object with low surface brightness ($4.5\times10^{-15}erg\,cm^{-2}\,s^{-1}\,arcsec^{-2}$ within a circular aperture with radius of 3.1″). The other outstanding feature in this region is the jet-like object located to the Southeast of the IRAS source (20:12:42.8 +41:03:43, 1950; labeled "jet" in figure 1), observed by Hodapp (1994) in a K′-band image. This object looks like an almost North-South oriented bipolar jet (length 19″ and PA= 172°), which is still visible on a continuum subtracted H_2 image. This emission apparently connects a central star with knot-like nebulosities at the two ends of the bipolar structure, having a surface brightness of about $4.6\times10^{-15}\,erg\,cm^{-2}\,s^{-1}\,arcsec^{-2}$ within a circular aperture of radius 3.1″(see figure 1, bottom panel).

The brighter NIR emission detected in our images (knots A, B and C in figure 2) has two main maxima, which approximately coincide with the lobes of the HCO^+ outflow, as shown in Fig. 3. This coincidence between the IR and HCO^+ emission was also noted by Cesaroni et al. (1997), who concluded that the IR emission is directly associated with the two lobes of the outflow.

Also quite remarkable is the fact that the IR emission NW of the IRAS source appears to be divided into two H_2-emitting, E-W directed ridges (condensations B and C of figure 2). Interestingly, a star is located at the Eastern end of each of these ridges. This can be appreciated by comparing the three panels of Fig. 2, and is confirmed by the spectroscopic data (described in the following section), which clearly show the stellar continua. In the region SE of the IRAS source (condensation A in figure 2), we detect a structure with two maxima, only one of which still remains in the continuum subtracted image (see figure 2), with a surface brightness of $2.1\times10^{-14}\,erg\,cm^{-2}\,s^{-1}\,arcsec^{-2}$ in the H_2 $\lambda2.121\,\mu m$ line.

3.2. Spectroscopic characteristics

From the three slit positions (1, $2a$ and $2b$) shown in Fig. 2(a), we can construct spatially integrated spectra for condensations B and C (NW of the IRAS source, see figure 2), and condensation A (SE of the IRAS source). These spectra are shown in Figs. 4 and 5. The integrated fluxes of the detected lines were extracted by fitting Gaussian profiles to each line, all of them required to have the same width (corresponding to that of the H_2 1-0 S(1) line). Table 2 lists the wavelength (Black & van Dishoeck, 1987), the energy of the upper level (Dabrowski 1984) and the measured fluxes of the detected H_2 lines for each object. The portions of the slit integrated for each object are shown in the upper panels of Figs. 4 and 5. For object C we have constructed a one-dimensional spectrum integrating over 11.1″ along slit 1 (see the upper panel in figure 4). The aperture includes the weak star to the E, indicated in Fig. 4, which contributes approximately 10% of the total emission at $\lambda\,2.121\,\mu m$. From the spectrum constructed with slits 2a+2b (see the upper panel of figure 5) we extracted spectra for condensations A and B, using 11.9″and 6.8″ apertures, respectively.

In condensation C, we have detected 6 low excitation H_2 lines (including both 1-0 and 2-1 vibrational transitions), and only 3 lines in the weaker condensations A and B. The measured 1-0 S(1)/2-1 S(1) line ratio for condensation C is 10.2 ± 0.5, which is comparable with the value of 10 expected for collisionally excited H_2 levels (see, e. g., Gredel et al. 1992; Gredel

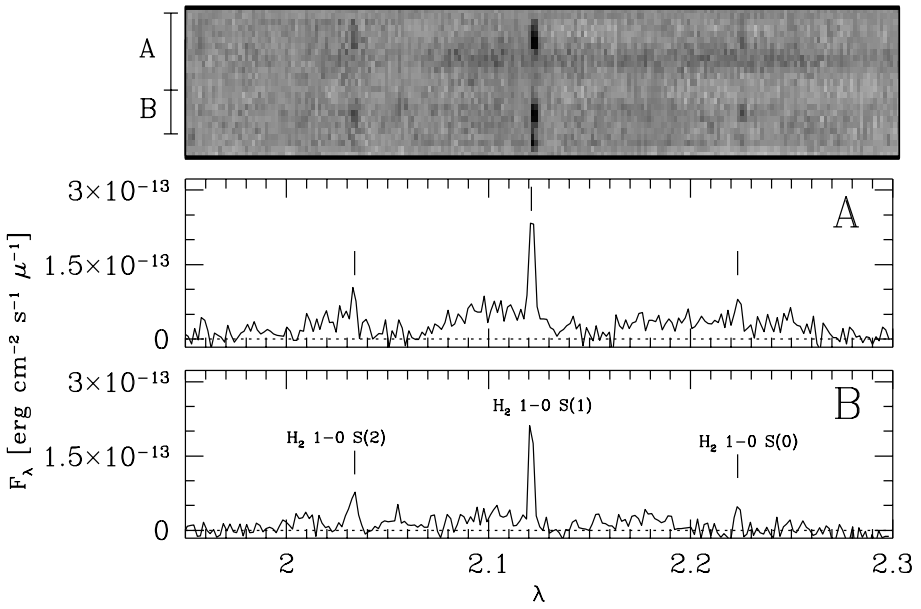

Fig. 5. *Top:* Grey-scale image of the long-slit K′-band spectrum obtained through slits 2a+2b. The apertures used to extract the spectra for objects A and B are indicated. The rest of emission corresponds to part of condensation labeled C and it is neglected. *Bottom:* Spectra of objects A and B, integrated over 11.9″ and 6.8″ along the slit, respectively.

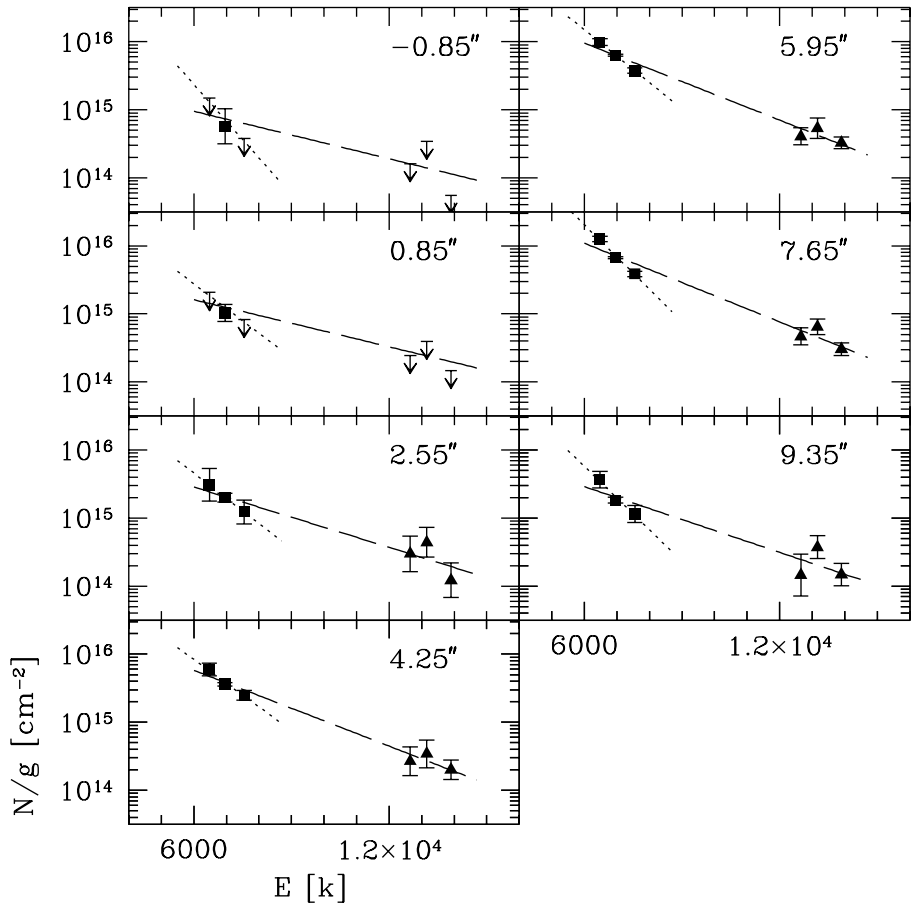

Fig. 6. Plot of column density for each level divided by statistical weight, derived from the intensities of lines in the K′-band spectra versus excitation energy of the upper level of each transition. Each H_2 excitation diagram has been constructed using spectra integrated in 1.7″ apertures along slit 1 in (see figure 2a) covering knot C. The position in arcsec along the slit is referred to the star on the slit (position zero) and we attach a position label in the upper right hand corner of each plot. The slope of the relationship between the parameters is inversely proportional to the excitation temperature. The points for the S(1) vibrational levels are plotted with solid squares and we have computed a "vibrational" temperature for these points (from the slopes of the dotted lines). The triangles correspond to the S(2) vibrational levels. The rotational temperature was computed including all of the H_2 lines (from the slopes of the dashed lines). In some cases errors are less than the size of symbols representing the S(1) vibrational levels.

1994). However, if we determine an upper limit for the 2-1 S(1) line flux over the spectra of the knots A and B, the estimated value of the 1-0 S(1)/2-1 S(1) line ratio is about 5, which would be somewhat low compared with the value for collisionally excited H_2 mentioned above.

We have also analyzed the spatially resolved line intensities, measured along the slit positions shown in Fig. 2(a). We computed the column densities $N(v, J)$ assuming that the lines are optically thin and using the spontaneous radiative decay probabilities from Turner et al. (1977). Figs. 6 (slit 1) and 7 ($2a + 2b$ slit) show the column densities as a function of the energy of

Table 2. Integrated H_2 line fluxes for objects A, B and C[a].

H_2 transition	λ $[\mu m]$	E(v', J') [K]	$F_{v'J'}$ $10^{-13}\ erg\ cm^{-2}\ s^{-1}$		
			A	B	C
1-0 S(2)	2.034	7550.8	1.23 (0.14)	1.52 (0.17)	2.02 (0.13)
2-1 S(3)	2.074	13902.0	< 0.50	< 0.50	0.94 (0.11)
1-0 S(1)	2.121	6957.2	3.09 (0.13)	3.95 (0.13)	6.85 (0.13)
2-1 S(2)	2.154	13161.4	< 0.50	< 0.50	0.52 (0.10)
1-0 S(0)	2.223	6476.8	0.91 (0.15)	1.06 (0.15)	1.81 (0.13)
2-1 S(1)	2.248	12650.7	< 0.50	< 0.50	0.67 (0.10)

[a] apertures used for integration of flux, A: 16.6, B: 10.2, C: 17.9 $arcsec^2$

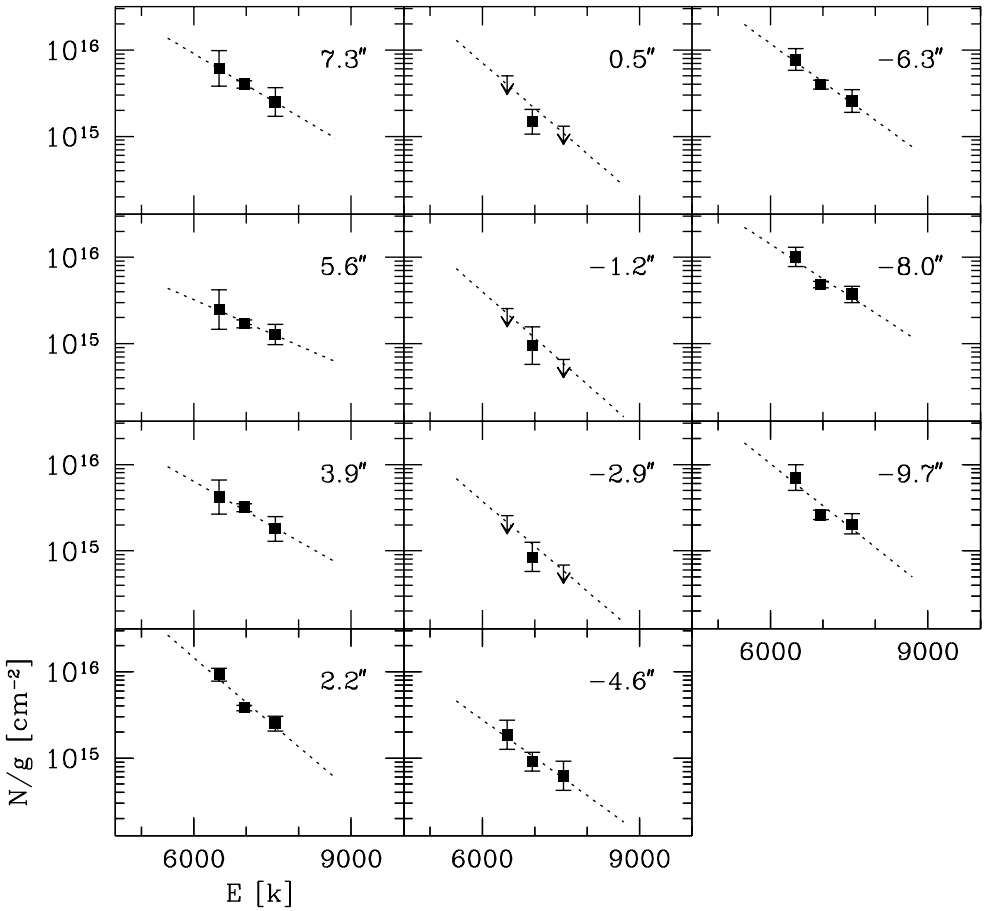

Fig. 7. H_2 excitation diagrams for the spectra obtained through slits 2a+2b, for different positions along the slit. The symbols and lines are the same as in Fig. 4. In this case the zero position corresponds to the position of the IRAS source projected on the spectrograph slit.

the upper level for the transition, deduced from the spatially integrated spectra. The successive panels correspond to spectra extracted in discrete positions along the spectrograph slits, integrating spatially over 1.7″. Where the lines were not clearly detected, we estimated an upper limit for the intensities and a column density was computed using these values. The slope obtained by fitting the points in a plot of $N(v, J)/g$ versus excitation energy is inversely proportional to the excitation temperature, where g is the corresponding level degeneracy. From these Figures, it is clear that we detect a rather strong spatial variability for the measured column densities. The derived values for different vibrational levels do not lie on a single smooth

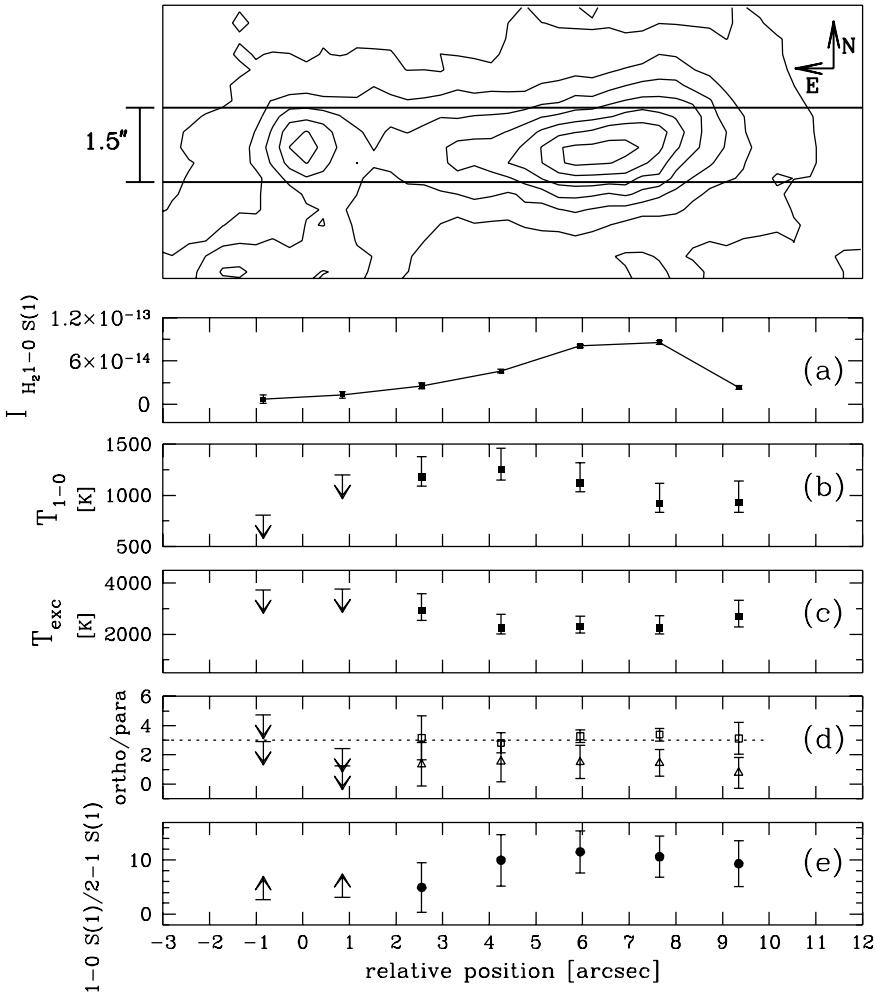

Fig. 8. *Top*: Contour plot of nebulosity C showing the position of the slit. The lower panels present the spatial variation along the slit of the parameters described below. These parameters were computed from consecutive spectra over $1.5'' \times 1.7''$aperture along the slit. The ordinate measures position as a function of distance from the star that lies close to the E end of the slit. (a) The spatial variation of H_2 λ 2.12 intensity in units of $erg\,cm^{-2}s^{-1}arcsec^{-2}$. (b) Spatial variation of the vibrational temperature of the K′-band spectrum, derived from the v = 1-0 transitions only. (c) Spatial variation of the excitation temperature, which has been computed using all of the H_2 lines identified in the K′-band spectrum. In both cases temperature increases slowly towards the position of the star, indicating a decreasing contribution by collisional excitation. (d) The spatial variation of the ortho/para ratio for the v = 1-0 level derived from the 1-0 S(1) and S(2) transitions (open squares) and from the 2-1 S(1) and S(2) transitions (open triangles). For the 1-0 lines, the ratio is near the LTE value of 3, as expected for collisional excitation, while the 2-1 lines yield low values for this ratio, which points towards fluorescent excitation. (e) Spatial variation of the 1-0/2-1 S(1) ratio. The ratio increases slowly along the slit with increasing distance from the star. Low values of this ratio reflect an important contribution of fluorescent excitation near the star, while values around 10 (obtained towards the W end of the slit) indicate collisional excitation.

curve, as would be expected for emission produced by a shock (Burton et al. 1990).

By fitting straight lines to the column density versus excitation energy diagrams, we determine two excitation temperatures: T_{exc} (obtained from fitting all of the observed lines) and T_{1-0} (obtained from a fit to the 1-0 transitions only). These temperatures are plotted as a function of position along the corresponding spectrograph slits in Figs. 8 (slit 1, covering condensation C) and 9 (slit 2*a*+2*b*, covering condensations A and B).

Along slit 1 (figure 8, panels (b) and (c)), we systematically have $T_{exc} > T_{1-0}$. This discrepancy between the two temperatures indicates that the excitation of the vibrational level $v = 2$ could have an important fluorescent component. This is also seen from the 1-0 S(1)/2-1 S(1) line ratio (figure 8(e)). We see two main regions, one where the line ratio has a mean value of 5 ± 5 (close to the star), and the other with a value $\approx 10 \pm 1.5$, and with a general tendency of decreasing line ratios towards the star. The behavior of this ratio close to the star is suspicious, because in this region the intensity of the lines decreases. In order check this behavior, we calculate the ratio over spectra integrated in only two bigger apertures which do not include the star. Using apertures of $3.4\ arcsec^2$ (centred on a position to 2.55″ W from the star) and $5.6\ arcsec^2$ (centred to 6.90″ W from the star). We find 1-0 S(1)/2-1 S(1) line ratios of 7.4 ± 4.0 and 11.6 ± 2.8, respectively. We therefore find that the tendency presented in Fig. 8 (e) for the 1-0 S(1)/2-1 S(1) line ratio remains. In the case of the vibrational temperature T_{1-0}, the region closer to the star has a mean temperature of about 1000 K, and it decreases slightly towards the W along condensation C (over an angular scale of 6″). On the other hand, the excitation temperature, T_{exc}, has an approximately constant value of ∼2400 K over the same angular scale. This value is somewhat low compared with the values observed in collisionally and fluorescent excited objects such as DR 2, where $T_{exc} \simeq 3000$ K using only 1-0 and 2-1 s(1) lines (Fernandes et. al 1997), and is also consistent with collisionally excited objects like HH 43, HH 120 and HH 99A in which $T_{exc} \simeq 2200$ K (Gredel 1994).

In all of the objects analyzed in this paper, the transitions between $v = 1$ and $v = 0$ are consistent with what is expected for levels populated in a thermalized gas at $T_{1-0} \sim 1000$ K. This temperature is lower than the ones found in the considered collisionally excited objects, where the excitation temperature estimated for the lowest transitions is of ~ 1900 K. The larger difference between T_{1-0} and T_{exc} found near the star at the E end of condensation C together with the lower 1-0 S(1)/2-1 S(1)

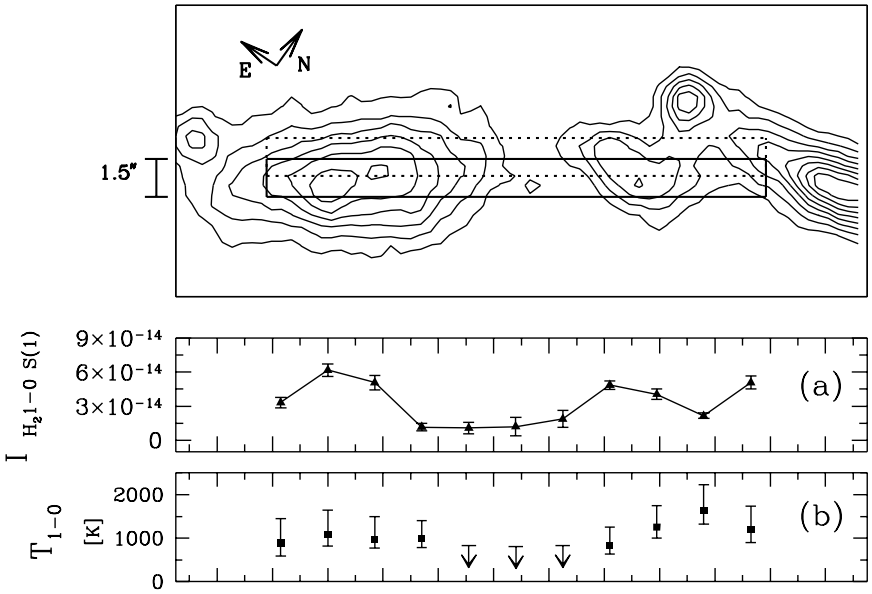

Fig. 9. Contour plot of the nebulosity located to the SE of the IRAS source showing the position of the spectrograph slits. The description of the parameters shown in the lower panels is the same as in Fig. 8. The zero of the ordinate corresponds the position of the IRAS source projected onto the spectrograph slit.

line ratio found in this region indicate that the H_2 molecules are excited by other processes besides collisions, like in DR 21 (Fernandes et. al 1997). A possible explanation for our results is that the star at the E of this condensation produces an UV field that significantly contributes to the excitation of the hydrogen molecules.

From the spectrum obtained through slits $2a$+$2b$ (figure 9) we see that condensations A and B, $T_{1-0} \sim 1100 \pm 500$ K, which is substantially smaller than a $T_{exc} \sim 3000$ K estimated using an flux upper limit for 2-1 lines determinate over each spectra. The T_{1-0} value is consistent with the mean temperature value founded for object C.

We also computed empirical values of the ratio of ortho-hydrogen to para-hydrogen, from ratios of available lines of even and odd J values in both vibrational levels. In panel (d) of Fig. 8 we plot the ortho/para ratio for condensation C, derived from the 1-0 S(1) and S(2) transitions (open squares) and the corresponding ratio from the 2-1 S(1) and S(2) transitions (open triangles). Along the slit the ortho/para ratio for $v = 1$-0 is near the LTE value of 3 (within error), as expected for collisional excitation. For the $v = 2$-1 transitions, we have lower values ($\leq 2.2 \pm 0.5$) for this ratio than the equilibrium value, which is characteristic of objects where there is a contribution by fluorescent excitation. For comparison, the ortho/para ratio estimated for the spectrum of the planetary nebula Hubble 12, where the H_2 lines is mainly excited by fluorescence, is 1.72 ± 0.17 (Ramsay et al. 1993). In condensation B the values of the ortho/para ratio estimated from the $v = 1$-0 transitions are about 3.1, which is consistent with the equilibrium value. In the case of condensation A we can only estimate lower limits for this ratio (~ 2).

From these results, we conclude that the H_2 excitation in condensation C has a strong fluorescent component in the Eastern region, close to the star that is observed at the E end of this condensation. Towards the W, the H_2 excitation along condensation C appears to be dominated by collisions (as supported by the high 1-0 S(1)/2-1 S(1) line ratio). On the other hand, the available data for the weak condensations A and B are not sufficient in order to propose the mechanism of molecular excitation more suitable in each case.

4. Discussion

The NIR emission of the region around the IRAS 20126+4104 source shows three main condensations (A, B and C, see figure 2), which are approximately aligned with the HCO^+ outflow observed by Cesaroni et al. (1997) (see figure 3). As shown by these authors, this outflow is centred quite precisely on the position of the IRAS source, and a compact molecular core is also observed at this central position. This clear source+bipolar outflow morphology argues strongly for an association of the IR emission with the outflow from the IRAS source (see Cesaroni et al. 1997).

The detailed analysis of the IR spectra carried out above shows that the situation is probably somewhat more complex. Our images and spectra show that the NW IR lobe is composed of two E-W elongated emission line condensations (B and C, see figure 2), with a star at the E end of each condensation. This morphology is somewhat curious, and might suggest a possible association of the two stars with condensations B and C.

We also find that the observed H_2 line ratios indicate that the excitation of the rotational-vibrational levels has a strong fluorescent component. Particularly interesting is the stratification of the line ratios along condensation C (see figure 2), which shows a 1-0 S(1)/2-1 S(1) line ratio indicating fluorescence towards the E end of the condensation (i. e., close to the position of the star), and a line ratio indicating collisional excitation towards the Western end of the condensation. The weighted mean ortho/para ratio for all the condensations, 2.3 ± 0.9, is lower than the equilibrium value of 3, consistent with a mixture of fluorescent and thermal excitation of H_2. The values of the ortho/para ratios measured for condensation C are consistent with objects such as NGC 7027, S106 and NGC 2023 (Tanaka et al. 1989)

and DR 21 (Fernandes et. al 1997) , which have "mixed" fluorescent plus collisional excitation, having significantly lower ratios for the $v = 2 - 1$ transitions than for the $v = 1 - 0$ transitions.

However, it is unclear whether or not these observations indicate an association of condensations B and C with the stars embedded at their Eastern tips. If such an association does exist, the emission of these condensations might partly be associated with radiative excitations by a UV continuum and/or Lyman-α emission from the circumstellar environment of these two stars. It might even be possible that these stars are illuminating the molecular gas associated with the outflow from the IRAS 20126+4104 source. However, the fact that the Western region of condensation C shows higher values for the 1-0 S(1)/2-1 S(1) line ratio (more consistent with collisional excitation of the levels of H_2) cannot be explained in straightforward manner with this interpretation.

To summarize, from our IR spectra we find partial evidence that the H_2 emission of condensations B and C (NW of IRAS 20126+4104) is associated with the stars embedded at the Eastern end of these condensations. On the other hand, these condensations also coincide spatially with the blue lobe of the HCO^+ outflow from IRAS 20126+4104 (Cesaroni et al. 1997), indicating a likely association of the H_2 emission with this flow.

The nature of the IR emission might be clarified with future, high spectral resolution spectroscopy. The resulting kinematic information would help to resolve the present, somewhat complex scenario.

Acknowledgements. This work was supported by grants from CONACYT and DGAPA (UNAM). S.A. acknowledges support from a DGAPA(UNAM) fellowship.

References

Ayala, S. Raga, A. Curiel, S. and Salas, L., 1997, in *Poster Proceedings of IAU Symposium n°182* "Herbig-Haro Flows and the Birth of Low Mass Stars", eds. F. Malbet and A. Castets, p. 5.
Black, J.H., and van Dishoeck, E.F. 1987, ApJ, 322, 412.
Bronfman L., Nyaman, L.A. and May, J., 1996, A&SS. 115, 81.
Burton, M.G., Hollenbach, D.J. and Tielens A.G.G.M., 1990, ApJ, 365, 620.
Cesaroni, R., Felli, M. and Walmsley, C. M., 1997, in *Poster Proceedings of IAU Symposium n°182* "Herbig-Haro Flows and the Birth of Low Mass Stars", eds. F. Malbet and A. Castets, p. 73.
Cesaroni, R., Felli, M., Testi, L., Walmsley, C. M., Olmi, L., 1997, A&A, in press.
Chernin, L. and Masson, C. 1993, ApJ, 414, 230.
Cruz-González, I., Carrasco, L., Ruiz, E., Salas, L., Strutskie, M., Meyer, M., Sotelo, P., Barbosa, F., Gutiérrez, L., Iriarte, A., Cobos, F., Bernal, A., Sánchez, B., Valdéz, J., Argüelles, S., and Conconi, P., 1994, in *Instrumentation in Astronomy VIII*, D.F. Crawford and E.R. Craine editors, Proc. SPIE 2198, p. 774. Rev. Mex. Astron. Astrofis., 29, 197.
Dabrowski, I. 1984, Canadian J. Phys., 62, 1639.
Elias, J.H., Frogel, J.A., Matthews, K. and Neugebauer, G., 1982, AJ, 87, 1029.
Fernandes, A. and Brand, P. 1995, MNRAS, 274, 639.
Fernandes, A., Brand, P. and Burton, M., 1995, Ap&SS, 233. 45.
Fernandes, A., Brand, P. and Burton, M., 1997, MNRAS, 290, 216.
Gredel, R., Reipurth, B. and Heathcote, S., 1992, A&A, 266, 439.
Gredel, R. 1994, A&A, 292, 580.
Hodapp, K., 1994 ApJS, 94, 615.
Martí, J. and Rodrí guez, L.F., 1997 in prep.
Molinari, S., Brand, J. Cesaroni, R. and Palla, F., 1996, A&A, 308, 573.
Raga, A.& Cabrit, S., 1993, A&A, 278, 267.
Raga, A. C., Cabrit, S., & Cantó, J. 1995, MNRAS, 273, 422.
Schwartz, R.D., Schultz, A.S.B., Cohen, M., Williams, P.D. 1995, ApJ, 446, 318.
Tanaka, M. Hasegawa, T., Hayashi, S.S., Brand, P.W.J.L. and Gatley, I. 1989, ApJ, 336, 207.
Turner, J. Kirby-Docken, K. and Dalgarno, A. 1977, ApJS, 25, 281.
Wilking, B.A, Blackwell, J.H. & Mundy, L.G., 1990 AJ, 100, 758.